

# Plasmonic shock waves and solitons in a nanoring

K. L. Koshelev,<sup>1,2,3</sup> V. Yu. Kachorovskii,<sup>1,3,4</sup> M. Titov,<sup>5</sup> and M. S. Shur<sup>6</sup>

<sup>1</sup>A. F. Ioffe Physico-Technical Institute, 194021 St. Petersburg, Russia

<sup>2</sup>ITMO University, 197101 St. Petersburg, Russia

<sup>3</sup>L. D. Landau Institute for Theoretical Physics, Kosygina street 2, 119334 Moscow, Russia

<sup>4</sup>Rensselaer Polytechnic Institute, 110, 8<sup>th</sup> Street, Troy, NY, 12180, USA

<sup>5</sup>Radboud University, Institute for Molecules and Materials, NL-6525 AJ Nijmegen, The Netherlands

<sup>6</sup>Center for Integrated Electronics, Rensselaer Polytechnic Institute, 110, 8<sup>th</sup> Street, Troy, NY, 12180, USA

We apply the hydrodynamic theory of electron liquid to demonstrate that a circularly polarized radiation induces the diamagnetic, helicity-sensitive  $dc$  current in a ballistic nanoring. This current is dramatically enhanced in the vicinity of plasmonic resonances. The resulting magnetic moment of the nanoring represents a giant increase of the inverse Faraday effect. With increasing radiation intensity, linear plasmonic excitations evolve into the strongly non-linear plasma shock waves. These excitations produce a series of the well resolved peaks at the THz frequencies. We demonstrate that the plasmonic wave dispersion transforms the shock waves into solitons. The predicted effects should enable multiple applications in a wide frequency range (from the microwave to terahertz band) using optically controlled ultra low loss electric, photonic and magnetic devices.

PACS numbers: 78.20.Ls, 78.67.-n, 73.23.-b, 75.75.-c

## I. INTRODUCTION

The feature size of modern electronic and photonic devices has dropped down to 10 nm. At such scales plasmonic excitations become a salient feature determining the device performance. This explains the recent increase of interest in plasmonics [1–7], the field which has to be further explored from the fundamental physics point of view [7].

Much of plasmonics physics could be captured by the hydrodynamic approach that is becoming increasingly relevant for electronic and spintronic devices due to fast improving quality of nanostructures. The first theories and measurements of the hydrodynamic effects on charge transport date to the early work by Gurzhi [8] and by Jong and Molenkamp [9]. A more recent interest to the field is driven by the emergence of the high-mobility nanostructures [10–18] and graphene [19–24] where the electron-electron collision-dominated transport regime can be reached.

The interest to the non-linear plasmon waves emerged in early 90s with exploiting the analogy between the “shallow water” hydrodynamics and that of the electron liquid in the two-dimensional (2D) gated systems. It was shown that the electron liquid could become unstable with respect to the excitations of tunable plasma oscillations [25]. Many other beautiful hydrodynamic phenomena such as choking of electron flow [26], nonlinear rectification of the plasma waves [27, 28] and the formation of the plasmonic shock waves [29] have been subsequently proposed. Possible applications of these phenomena to the plasma-wave electronics were intensely discussed (see reviews [30, 31]). In particular, much attention has been recently paid to the generation of the plasmonic oscillations in the field-effect transistors (FETs) for realizing tunable THz emitters or detectors [30, 31].

The detector responsivity is enhanced dramatically in the presence of a  $dc$  current [32]. It can be also enhanced by making artificial periodic structures such as FET arrays and periodically grating gates [33–37]. Such plasmonic crystals have already demonstrated excellent performance as THz de-

tectors [38–42] in a good agreement with the theory [43–46]. THz emission from the grating gate structures have been also recently reported [47, 48].

Having a non-zero  $dc$  photovoltaic response in a single FET requires an inversion asymmetry which can be created by boundary conditions [25]. Plasmonic crystals would require an inversion asymmetry within the unit cell of the crystal. Such an asymmetry can be induced by a ratchet effect (see review paper [49] and the references therein). The latter is also strongly enhanced by plasmons [50].

Here we explore another system enabling a greatly enhanced coupling between the THz radiation and plasmonic excitations – a ballistic nanoring. Such a system has a number of advantages compared to a single FET. First of all, an inversion asymmetry is not required in this case because of the nanoring multi-connected geometry [51–58].

More importantly, we now predict that the plasmonic resonances in a high-quality nanoring can be much sharper as compared to a FET. Indeed, the dissipation in the contacts and coupling with the ungated regions in FETs leads to essential weakening of plasmonic resonances. In the nanorings, these deleterious effects are completely avoided. The coupling can be further enhanced by fabricating nanoring arrays.

We predict that the excitation of the plasmonic waves by a circularly polarized radiation leads to a resonant optical rectification effect – a large diamagnetic circulating  $dc$  current that manifests itself as a magnetic moment of the nanoring. When the radiation intensity exceeds a critical value, the plasmonic waves transform into the shock waves (SW) that might further develop into multiple solitons (a similar effect was recently predicted for nonlinear waves in the Luttinger liquid [59, 60]). In this regime, the system functions as an efficient emitter of the high frequency radiation harmonics. One possible application of this effect is to use the plasmonic SWs for the frequency multiplication transforming a circularly polarized resonant GHz waves into a number of well resolved peaks at THz frequencies.

Circulating current in a nanoring gives rise to the inverse

Faraday effect (IFE), which is the excitation of helicity-sensitive magnetic moment by a circularly polarized light [61–64]. The IFE has been widely discussed in connection with ultrafast magnetisation dynamics [63–66]. The quantum IFE in nanorings [51–58] and in a chaotic cavity [67] has also been discussed. Remarkably, the plasmonic IFE described below is based on quasiclassical mechanism and, consequently, orders of magnitude stronger than the corresponding quantum phenomenon.

The closed rings have an important advantage compared to the ring-split resonators (see Ref. [68] and reference therein). The ring-split resonators can create large values of optically induced *alternating* magnetic field, but can not conduct circulating dc current, and, consequently, do not produce a *constant* magnetic field. In contrast, as we discuss below, the excitation of a closed ring by a circularly polarized radiation might result in quite large values of a constant magnetic field (on the order of a Gauss or even larger for the stacked rings and ring arrays). Similar phenomena should occur in metallic films perforated with hole arrays [64].

## II. MODEL

The electron liquid in a multi-channel nanoring subject to a circularly polarized radiation can be described by the hydrodynamic equations for the electron concentration (per unit length)  $N$  and the hydrodynamic velocity  $V$ . The approach is justified in high-quality rings where the electron-electron collisions dominate.

For a nanoring of the radius  $R$  the equations take the form,

$$\frac{\partial N}{\partial t} + \frac{\partial(NV)}{\partial x} = 0, \quad (1)$$

$$\frac{\partial V}{\partial t} + V \frac{\partial V}{\partial x} - \eta \frac{\partial^2 V}{\partial x^2} = -\gamma V - \frac{\partial \Phi}{\partial x} + \frac{eE_0}{m\varepsilon} \sin \theta, \quad (2)$$

where  $x$  is the coordinate along the ring,  $E_0$  is the amplitude and  $\omega$  is the frequency of circularly polarized radiation,  $\eta$  is the kinematic viscosity of electron liquid,  $m$  is the effective electron mass,  $\gamma$  is the friction due to scattering off impurities,  $\varepsilon$  is dielectric constant and

$$\theta = x/R - \omega t. \quad (3)$$

The electrostatics of a thin nanoring is solved by (see Appendix A)

$$\Phi = \frac{e^2}{m\varepsilon} \left[ (N - N_0)\Lambda + d^2 \frac{\partial^2 N}{\partial x^2} \right] = s^2 \left[ n + \frac{d^2}{\Lambda} \frac{\partial^2 n}{\partial x^2} \right], \quad (4)$$

where  $\Lambda = \ln(d^2/a^2)$ ,  $N_0 = \pi a^2 n_{3D}$ ,  $\pi a^2$  is the nanoring cross-section,  $n_{3D}$  is the equilibrium value of the 3D electron concentration,  $d$  is the screening radius ( $a \ll d \ll R$ ),

$$n = (N - N_0)/N_0 \quad (5)$$

is the relative dimensionless concentration, and

$$s = \sqrt{\frac{e^2 N_0 \Lambda}{m\varepsilon}} \quad (6)$$

is the plasma wave velocity, respectively [see Eq. (7) below] which might be tunable by the gate voltage.

In Eq. (4), we neglect the pressure of the electronic liquid assuming that  $s$  is large compared to the Fermi velocity. We also neglect the thermoelectric forces (compared to  $\partial \Phi / \partial x$ ) that allows us to decouple Eqs. (1) and (2) from the heat transfer equation [50]. Finally, we neglect the dependence of  $\eta$  on  $N$  (setting  $\eta(N) \approx \eta[N_0]$ ) and regard  $N$  to be smooth on the scale of  $d$ , thus keeping the main logarithmic contribution to the Coulomb potential and the leading correction to it (see Appendix A). The latter describes a weak plasmonic dispersion. The subtle question is related to the boundary conditions at the surface of the ring. The often used no-slip condition  $V = 0$  would result in the Poiseuille flow and, consequently, in a relatively large resistance caused by viscosity. On the other hand, recent technology allows for fabricating quantum wires and rings of an extremely high quality. This implies that the friction originating at the surface of the ring might be quite low and insufficient to drive the ring into the Poiseuille regime. Therefore, in the derivation of Eqs. (1), we fully neglected this friction, so that  $N$  and  $V$  depend only on  $x$ . A more general case of an arbitrary strong surface friction is briefly discussed in Appendix B.

## III. LINEAR REGIME

When the radiation intensity is small, the Eqs. (1,2) can be linearized. In the absence of radiation and for  $\eta = 0, \gamma = 0$ , plasma waves propagating in a ring have the linear spectrum

$$\omega(k) = sk, \quad (7)$$

where  $s$  is given by Eq. (6) [here we neglect the small dispersion due to the second term in the square brackets in Eq. (4)]. The wave vectors are quantized:

$$k_n = n/R, \quad (8)$$

where  $n$  is the integer number ( $n \neq 0$ ). Both friction  $\gamma$  and viscosity  $\eta$  lead to damping of the waves similar to the damping effects in FETs [25].

A weak external radiation field impinging on the ring couples to the electronic fluid and excites linear plasmonic oscillations with the fundamental frequency

$$\omega_0 = \frac{s}{R} = \frac{a}{R} \sqrt{\frac{\pi e^2 \Lambda n_{3D}}{m\varepsilon}}. \quad (9)$$

For a circularly polarized radiation, the oscillations are rectified to produce the *dc* circulating current that peaks at the plasmonic resonant frequencies:

$$I_{dc} = e \langle NV \rangle, \quad (10)$$

where the brackets stand for the time average. The direction of the current is determined by the radiation helicity (below we put  $\omega > 0$ ):

$$I_{dc}(\omega) = -I_{dc}(-\omega). \quad (11)$$

We now introduce the rescaled quantities

$$J = I_{dc}/eN_0R, \quad v = V/R, \quad (12)$$

$$\varkappa = \eta/R^2, \quad \beta = \omega_0^2 d^2 / \Lambda \omega R^2, \quad (13)$$

that we respectively refer to as current, velocity, viscosity and dispersion.

Solving the linearized equations, we find in the resonance approximation, i.e. for  $\delta = \omega_0 - \omega \ll \omega_0$ :

$$v = \omega n = \frac{eE_0}{mR\varepsilon} \text{Im} \frac{e^{i\theta}}{\varkappa + \gamma + i(2\delta - \beta)}, \quad (14)$$

$$J = \langle nv \rangle = \frac{1}{2\omega} \left( \frac{eE_0}{mR\varepsilon} \right)^2 \frac{1}{(\varkappa + \gamma)^2 + (2\delta - \beta)^2}. \quad (15)$$

Here  $\beta \approx \omega_0 d^2 / \Lambda R^2$  for  $\delta \ll \omega_0$ . Thus, the *dc* response is given by a simple Lorentzian that peaks at the plasmonic frequency with a small dispersion-induced shift  $\beta$  and broadened by disorder and viscosity.

For the typical parameters  $n_{3D} = 10^{17} \text{cm}^{-3}$ ,  $m = 10^{-28} \text{g}$ ,  $\varepsilon = 10$ ,  $a = 10^3 \text{\AA}$ ,  $d = 3 \cdot 10^3 \text{\AA}$ , and  $R = 10^4 \text{\AA}$ , we find that  $\omega_0/2\pi \simeq 0.2 \text{THz}$  and

$$\omega_0/\beta \approx 25. \quad (16)$$

In the electron collision-dominated regime,  $\eta$  is on the order of  $v_F^2 \tau_{ee}$ , where  $\tau_{ee}^{-1}$  is the scattering rate due to the electron-electron collisions estimated as

$$\hbar/\tau_{ee} \sim T^2/E_F. \quad (17)$$

Thus, for  $T = 30^\circ \text{K}$ , we estimate  $\varkappa \approx 0.3 \cdot 10^{11} \text{s}^{-1}$ . Therefore, for a high-quality nanoring ( $\gamma < \varkappa$ ), the quality factor of plasmonic resonance is very high

$$\omega_0/\varkappa \approx 80. \quad (18)$$

#### IV. NONLINEAR REGIME.

For larger radiation intensities, the non-linear terms in Eqs. (1,2) become increasingly important. Figs. 2 and 3 show the results of the numerical analysis of Eqs. (1,2) using a finite element method (see Appendix E). We find that, at sufficiently long times, the solution is stationary in the rotating reference frame. No chaotic or turbulent behavior is obtained. The results obtained numerically at long time can be reproduced analytically by analyzing the automodel solutions with  $n = n(\theta)$ ,  $v = v(\theta)$  that satisfy the neutrality condition  $\langle n \rangle = 0$ , where the angular brackets now stand for the averaging over the angle  $\theta$ . In this case, the Eq. (2) imposes the constraint

$$\langle v \rangle = 0. \quad (19)$$

Integration of Eq. (1) accounting for this constrain leads to the relation

$$J = -\omega n + (1 + n)v. \quad (20)$$

For sufficiently small velocities,  $v \ll \omega$ , we, therefore, obtain the charge density

$$n = (J - v)/(v - \omega) \approx v/\omega + v^2/\omega^2 - J/\omega, \quad (21)$$

which can be substituted into Eq. (1) to obtain the equation

$$\frac{\partial}{\partial \theta} \left[ 2v\delta + \frac{3}{2}v^2 - \varkappa \frac{\partial v}{\partial \theta} + \beta \frac{\partial^2 v}{\partial \theta^2} \right] = -\gamma v + \frac{eE_0}{mR\varepsilon} \sin \theta. \quad (22)$$

that holds in the resonant approximation. The electric current is found from the solution of Eq. (22) as

$$J = \langle nv \rangle \approx \langle v^2 \rangle / \omega. \quad (23)$$

Since both the viscosity and disorder suppress resonant behavior in a similar way [see Eq. (15)], we consider, for simplicity, the case  $\gamma = 0$ . (Importantly, the limit  $\gamma \rightarrow 0$  should be taken with care, since any small but finite  $\gamma$  guarantees the constraint  $\langle v \rangle = 0$  that follows immediately from averaging Eq. (22) over the angle  $\theta$ . In what follows we neglect the term  $\gamma v$  in Eq. (22) but respect the constraint.) We integrate Eq. (22) over the angle and introduce the variables

$$q = 3v/2 + \delta, \quad F = 3eE_0/2mR\varepsilon \quad (24)$$

to find

$$\beta \ddot{q} + \varkappa \dot{q} = q_0^2 - q^2 - F \cos \tau, \quad (\tau = -\theta) \quad (25)$$

where

$$q_0^2 = \langle q^2 \rangle \quad (26)$$

is the integration constant which should be found self-consistently and  $\dot{q} = dq/d\tau$ . The Eq. (25) coincides with the Newton equation of motion for a particle with the "mass"  $\beta$  oscillating in a classical cubic potential

$$U(q) = q^3/3 - q_0^2 q \quad (27)$$

under the action both of the external dynamic force  $-F \cos \tau$  and the "friction force"  $-\varkappa \dot{q}$ . The motion is further constrained by two conditions:

$$q(\tau) = q(\tau + 2\pi), \quad (28)$$

$$\langle q \rangle = \delta. \quad (29)$$

The potential  $U(q)$  has two stationary points (see Fig. 1):  $q = q_0$  (stable minimum) and  $q = -q_0$  (unstable maximum). The corresponding energies are given by  $U(q_0) = -2q_0^3/3$  and  $U(-q_0) = 2q_0^3/3$ . For small values of  $F$ , the particle undergoes linear oscillations around the stable point. Expanding  $q_0^2 - q^2 \approx 2q_0(q_0 - q)$  in the r.h.s. of Eq. (25) and solving the corresponding linear equation one readily reproduces Eq. (14). In this case,  $q_0 \approx \delta$ .

Let us fix  $\delta$  at a certain value and increase  $F$  to drive the system into a nonlinear regime. First, we assume that both viscosity and dispersion are absent ( $\varkappa = \beta = 0$ ). Then, Eq. (25) has two solutions:

$$q(\tau) = \pm \tilde{q}_0(\tau), \quad \tilde{q}_0(\tau) = \sqrt{q_0^2 - F \cos \tau}, \quad (30)$$

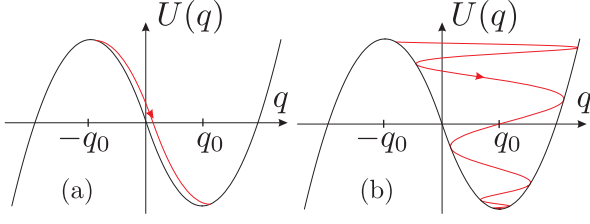


FIG. 1: The effective potential (black lines) and solutions (red lines) of Eq. (25) for  $\beta \ll \beta_0$  and (a) for  $\beta_0 < \beta < \varkappa$  (b) for  $F > F_{\text{cr}}$ .

where  $\tilde{q}_0(\tau)$  indicate the positions of extrema of dynamical potential

$$\tilde{U} = U(q) + Fq \cos \tau = q^3/3 - \tilde{q}_0^2 q. \quad (31)$$

Since  $\langle q \rangle = \delta$ , the choice of a solution is fixed by the sign of  $\delta$ . To be specific we let  $\delta > 0$  below. Upon angle averaging the dependence of  $q_0$  on  $F$  and  $\delta$  is given implicitly by

$$\delta = \int \frac{d\tau}{2\pi} \sqrt{q_0^2 - F \cos \tau}. \quad (32)$$

This equation has a solution only for  $F < F_{\text{cr}}$ , where

$$F_{\text{cr}} = \pi^2 \delta^2 / 8. \quad (33)$$

The linear regime is reproduced in the limit  $F \ll F_{\text{cr}}$  (see Appendix C 1). The corresponding solution for  $v(\theta)$  is shown by a solid line in Fig. 2a. The dashed line corresponds to a negative solution in Eq. (30). For  $F > F_{\text{cr}}$  Eq. (32) breaks down and the velocity profile is discontinuous (detailed calculation in Appendix C 1), i.e. a step (SW front) appears at a certain point  $\tau = \tau_0$ . The amplitude of the step is given by  $2\tilde{q}_0(\tau_0)$ , where

$$\cos(\tau_0/2) = \sqrt{F_{\text{cr}}/F}, \quad \tilde{q}_0(\tau_0) = \sqrt{2(F - F_{\text{cr}})}. \quad (34)$$

The amplitude of the SW front increases monotonously with  $F$  and is given by  $\sqrt{8F}$  in the limit  $F \gg F_{\text{cr}}$ . In this limit, the front is located at  $\tau_0 \approx \pi$  (see Fig. 2d).

### A. Finite viscosity.

Let us now switch to the case of a finite viscosity while still assuming that  $\beta = 0$ . Viscosity tends to regularize the discontinuity in the solution in such a way that the SW front is smeared out on a finite time scale

$$\delta\tau = \varkappa / 2\tilde{q}_0(\tau_0) \sim \varkappa / \sqrt{F - F_{\text{cr}}}. \quad (35)$$

Fig. 1a shows the corresponding motion in the effective potential. During the time interval  $\delta\tau$  a particle propagates from the unstable point to a stable one due to the friction force in Eq. (25). For sufficiently small viscosity, when  $\delta\tau \ll 1$ , one can let  $F \cos \tau \approx F \cos \tau_0$  within the front width. Then, Eq. (25) is solved exactly and we find that the smeared step is well described by the SW solution

$$q(\tau) = \sqrt{2(F - F_{\text{cr}})} \tanh \left[ \sqrt{2(F - F_{\text{cr}})} (\tau - \tau_0) / \varkappa \right]. \quad (36)$$

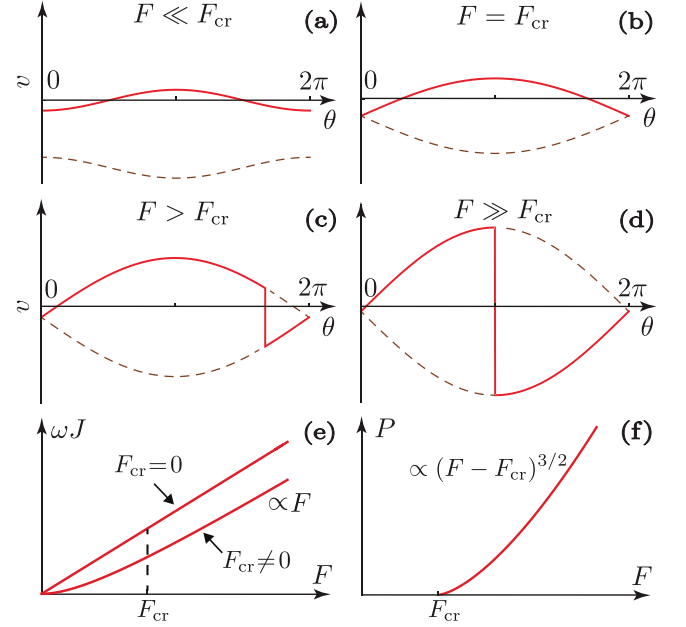


FIG. 2: Velocity  $v$  and concentration  $n \approx v/\omega$  profiles for different  $F$  (a-d). Solid and dashed lines in (a,b) correspond to positive and negative solutions of Eq. (30). At  $F = F_{\text{cr}}$ , these solutions touch each other (b). Critical amplitude  $F_{\text{cr}}$  corresponds to a formation of the SW front. For  $F > F_{\text{cr}}$  there is a jump between positive and negative solutions of Eq. (30) shown in the panels (c) and (d) by dashed lines. The panels (e) and (f) show the dependence of the current  $J$  and the dissipated power  $P$  on  $F$  for  $\beta = 0$  and  $\varkappa \rightarrow 0$ .

A simple analysis yields the electric current  $J$  and the dissipated power

$$P = e \langle NV E_0 \sin \theta \rangle \quad (37)$$

per unit volume in the limit  $\varkappa \rightarrow 0$  [see Fig. 2(e,f)]. We find

$$F < F_{\text{cr}} : J = \frac{\pi^2 F^2}{144 \omega F_{\text{cr}}}, \quad P \equiv 0, \quad (38)$$

$$F > F_{\text{cr}} : J = \frac{4}{9\omega} \left( F - \frac{8F_{\text{cr}}}{\pi^2} \right), \quad P = C(F - F_{\text{cr}})^{3/2} \quad (39)$$

where  $C = 16\sqrt{2}mN_0/81\pi$  is independent of viscosity. Remarkably, the current remains finite even for  $\varkappa = \gamma = 0$ , which implies that it has a diamagnetic nature. Even more interesting, the power  $P$  remains finite above the threshold,  $F > F_{\text{cr}}$ . In this regime, the energy dissipation occurs at the front of the SW in the region with the width on the order of  $\varkappa$  and is proportional to  $\varkappa v \partial^2 v / \partial \theta^2 \propto 1/\varkappa$ . As a result,  $\varkappa$  drops out from the expression for total dissipation [69]. It is worth stressing that the strong-coupling result of Eq. (39) is essentially non-perturbative.

Using the Fourier transform

$$v = \sum_n v_n \exp(in\theta), \quad (40)$$

we observe that the dependence of  $v_n$  changes qualitatively at the SW emergence. For  $F < F_{\text{cr}}$ , the high order harmonics exponentially decay with  $n$ ,  $v_n \propto \exp(-an)$ , where



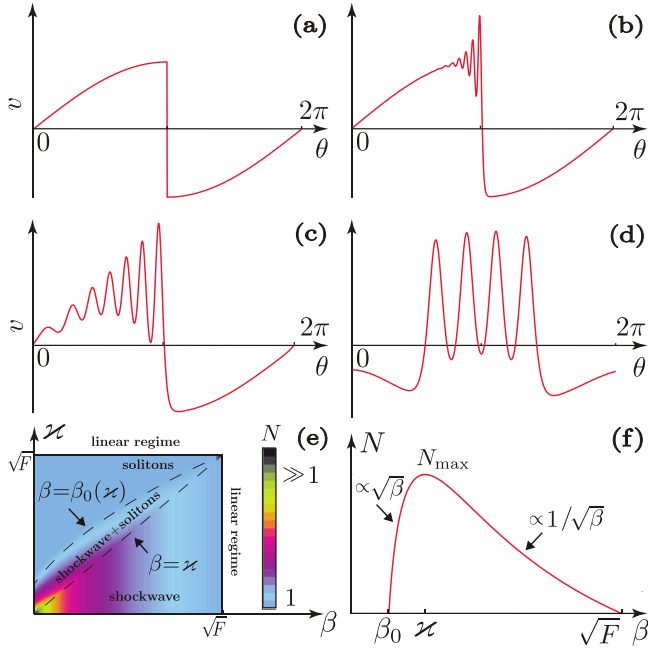


FIG. 3: Evolution of the solution showing the emergence of the solitons at the SW front with increasing dispersion coefficient  $\beta$  at  $F \gg F_{cr}$  and  $\varkappa \ll \sqrt{F}$ : (a)  $\beta \ll \beta_0$ , (b)  $\beta \gtrsim \beta_0$ , (c)  $\beta \sim \varkappa$ , (d)  $\varkappa/\delta\tau \gg \beta \gg \varkappa$ . The phase diagram in the dispersion-viscosity plane (e), where the color indicates the number of solitons  $N$ , and the dependence of the number of solitons  $N$  on the dispersion parameter  $\beta$  (f).

$a \propto F_{cr} - F$  at  $F \rightarrow F_{cr}$  (this estimate holds with an exponential precision). Exactly at the threshold, one finds  $v_n \propto 1/n^2$ , while for  $F > F_{cr}$ , the decay of harmonics  $v_n$  is very slow,  $v_n \propto 1/n$ , which is the consequence of the step-like behavior of the solution [see Figs. 2(c,d)]. This power-law dependence is valid for  $n < 1/\delta\tau$ . The higher harmonics are exponentially suppressed because of the finite front width of the SW. Hence, generation of the SW leads to a large increase of the excited harmonics.

With increasing viscosity  $\varkappa$ , the SW front smears, the non-linear oscillations are suppressed and evolve into linear ones for  $\varkappa \gg \sqrt{F}$ . The exact solution to Eq. (25) for arbitrary  $\varkappa$  (but  $\beta = \gamma = 0$ ) is presented in Appendix C 2.

### B. Generation of solitons due to the dispersion of plasma velocity.

Let us now assume that  $F > F_{cr}$ , fix  $\varkappa$  at a sufficiently small value (such that  $\delta\tau \ll 1$ ) and study what happens with increasing the dispersion coefficient  $\beta$ . The evolution of solutions is illustrated in Fig. 3(a-d). We see that dispersion leads to a formation of solitons on the SW front. This process can be simply understood by analyzing the mechanical analogy described above.

Since  $\beta$  is responsible for inertia in Eq. (25) it leads to the transformation of the decaying solution (see Fig. 1a) into an oscillatory one (see Fig. 1b). For a finite, but sufficiently small

$\beta$  ( $\beta \ll \varkappa$ ), the SW front remains sharp and one can still assume  $F \cos \tau \approx F \cos \tau_0$  within the front width. Then, the characteristic scales of the problem can be understood from the analysis of Eq. (25) linearized near the stable point:

$$\beta \ddot{\delta q} + \varkappa \dot{\delta q} + (\varkappa/\delta\tau) \delta q = 0, \quad (41)$$

where

$$\delta q = q - \tilde{q}_0(\tau_0). \quad (42)$$

By searching for the solution of this equation in the form  $\exp[\lambda\tau]$  we find

$$\lambda = -(\varkappa/2\beta)(1 \pm \sqrt{1 - \beta/\beta_0}), \quad (43)$$

where  $\beta_0 = \varkappa\delta\tau/4 \ll \varkappa$ .

For  $\beta \ll \beta_0$ , we find two exponentially decaying solutions, the slowest one corresponds to  $\lambda \approx -1/\delta\tau$ . In this case, the dispersion does not play any essential role as seen from Fig. 3a (for simplicity, in Fig. 3 we consider  $F \gg F_{cr}$ ). The finite viscosity broadens the SW front on the scale of  $\delta\tau$ .

Solitons start to form for  $\beta > \beta_0$ . In this case, the exponent  $\lambda$  acquires an imaginary part and the oscillations appear on top of the smeared wave front as seen in Fig. 3b. (Similar effects also arise in the Luttinger liquids [59, 60]). For the case  $\beta_0 \ll \beta \ll \varkappa$ , we find two rapidly oscillating and slowly decaying solutions. The number of oscillations during the decay from the unstable to the stable point (the number of solitons  $N$ ) can be estimated as the ratio of imaginary part of  $\lambda$  to its real part yielding

$$N \sim \sqrt{\beta/\beta_0}. \quad (44)$$

This number increases with  $\beta$  up to  $\beta \sim \varkappa$  (see Fig. 3c).

When  $\beta$  becomes larger than  $\varkappa$  both solutions do not decay for the whole oscillation period of the external force  $0 < \tau < 2\pi$ . As the result, for  $\beta \gg \varkappa$  viscosity can be fully neglected and transition from the unstable point to the stable one is due to adiabatically slow variation of the potential. The number of oscillations in this case can be estimated as

$$N \sim \text{Im}\lambda \sim \varkappa/\sqrt{\beta\beta_0}. \quad (45)$$

The corresponding solution is shown in Fig. 3d.

This analysis suggests that the maximal value of solitons is achieved for  $\varkappa \sim \beta$  with

$$N_{\max} \sim \sqrt{\varkappa/\beta_0} \propto 1/\sqrt{\delta\tau}. \quad (46)$$

Different regimes are summarized in Fig. 3e in the coordinates  $(\varkappa, \beta)$ . The dependence of  $N$  on  $\beta$  is plotted in Fig. 3f. A more detailed analytical study of the limit  $\beta \gg \varkappa$  is presented in Appendix D.

## V. RESULTS AND CONCLUSION

Let us briefly discuss the conditions to be met for observing the strongly non-linear regimes discussed above. Exactly at the resonance,  $\delta = 0$ , the non-linear behavior occurs

for  $\sqrt{F} > \kappa, \beta$  (see Fig.3e). The condition boils down to  $E_0 > 10^3$  V/cm for parameters used above in the estimation of the quality factor. The corresponding field amplitude can be easily reached in modern sources of GHz and THz radiation. Such or much higher fields are even easier to realize in the pulsed regime of operation (with the minimum pulse width only limited by the period of the electromagnetic wave.)

To conclude, we demonstrated that circularly-polarized radiation induces a strong diamagnetic  $dc$  current in a nanoring, which is dramatically enhanced in the vicinity of plasmonic resonances. For the ballistic rings, the quality factor of the resonances can be as high as  $10 \div 100$ . When the amplitude of the external field exceeds a critical value  $F_{cr}$  shock waves and/or solitons are formed. In this regime, the current and magnetic moment grow linearly with the field amplitude and a large number of harmonics is generated.

The discovered enhancement of the diamagnetic current by the plasmonic resonance should enable numerous applications of ballistic nanorings and nanoring array including, but not limited to, the electric field control of magnetic forces, and new generation of highly efficient low loss switches operating from microwave range to the upper bound of the THz range.

### Acknowledgments

We thank I. Gornyi, A. Kimel, A. Mirlin, D. Polyakov, and I. Protodopov for stimulating discussions. The work of M.T. was supported by the EU Network FP7-PEOPLE-2013-IRSES Grant No 612624 “InterNoM” and by Dutch Science Foundation NWO/FOM 13PR3118. The work of K.L.K. and V.Yu.K. was supported by Russian Science Foundation (grant No. 16-42-01035)

### Appendix A: Electrostatic potential

We start by deriving the Eq. (4) of the main text. Let us consider electrostatic force (per unit mass) created by electrons distributed along the ring with the concentration  $N = N(x)$ . We assume that the Coulomb interaction is screened on the scale  $d$  such that  $d \ll R$ . Then, in the limit of infinitely thin wire, the force per unit mass acting on the electric flow at the point  $x$  can be written as  $-\partial\Phi/\partial x$ , where

$$\Phi = \frac{e^2}{m\varepsilon} \int dx' [N(x') - N_0] \frac{\exp(-|x - x'|/d)}{|x - x'|}. \quad (\text{A1})$$

The integral entering Eq. (A1) diverge logarithmically at  $x' \rightarrow x$ . This divergency is regularized by taking into account a finite width  $a$  ( $a \ll d$ ) of the ring. Assuming that  $N(x)$  changes slowly on the scale  $d$  we may cast the electron concentration in the form  $N(x') \approx N(x) + N'(x)(x - x') + (1/2)N''(x)(x - x')^2$ . Substituting this equation into Eq. (A1) and performing (with logarithmic precision) the integration over  $x'$  we arrive at Eq. (4) of the main text.

### Appendix B: Linear solution for finite friction at the surface

In this section, we briefly discuss the effect of the surface friction in the linear regime, i. e. for the linear plasmonic excitations.

The surface friction leads to a inhomogeneous distribution of the velocity and concentration in the radial direction. In the resonance approximation, linearized velocity can be written as  $v = v_1(r) \exp(i\theta) + \text{h. c.}$ , where  $v_1$  yields the equation

$$v_1 [i(2\delta - \beta) + \kappa + \gamma] - \kappa \frac{R^2}{r} \frac{\partial}{\partial r} \left( r \frac{\partial v_1}{\partial r} \right) = \frac{eE_0}{2imR\varepsilon}. \quad (\text{B1})$$

Here  $r$  is the radial coordinate such that  $0 < r < a$ . Since our calculations have illustrative character, we do not distinguish here between bulk and shear viscosity, characterizing the electron liquid by a single viscosity coefficient  $\kappa$ . We further assume that the friction force is proportional to the velocity and can be modeled by a delta-function potential on the surface of the ring,  $V f \delta(r - a)$ , where  $f$  is a certain coefficient. In this model we find the boundary condition to Eq. (B1) as

$$\left. \frac{\partial v_1}{\partial r} \right|_{r=a} = -k v_1, \quad (\text{B2})$$

where  $k = f/\eta$ . For sufficiently large radius  $R$  such that  $a^2 |i(2\delta - \beta) + \kappa + \gamma| / \kappa R^2 \ll 1$ , the solution to Eq. (B1) with the boundary condition of Eq. (B2) reads

$$v_1 \approx \frac{eE_0}{2imR\varepsilon} \frac{1 + k(a^2 - r^2)/2a}{\tilde{\kappa} + \gamma + i(2\delta - \beta)}, \quad (\text{B3})$$

where  $\tilde{\kappa} = \kappa(1 + 2kR^2/a)$ . For the limit

$$k \ll \frac{a}{R^2}, \quad (\text{B4})$$

or, equivalently, for  $f \ll \kappa a$ , we restore Eq. (14) of the main text. Hence, the inequality (B4) represents a criterium for neglecting the friction force. For larger values of  $k$  the friction would modify our results. As far as  $a/R^2 \ll k \ll 1/a$  the modification is simply reduced to replacing  $\kappa$  in Eq. (14) with a large constant  $\tilde{\kappa} \gg \kappa$ . For even larger values,  $k \gg 1/a$ , one obtains the dynamical Poiseuille flow in which velocity goes to zero on the nanoring surface.

### Appendix C: Exact solutions

#### 1. Exact solution at $F \ll F_{cr}$ and $F > F_{cr}$ for $\gamma = \kappa = \beta = 0$ .

The linear regime is analyzed by expanding Eqs. (30) and (32) in  $F$ . Simple analysis yields

$$q_0 \approx \delta + \frac{F^2}{16\delta^3}, \quad q \approx \delta - \frac{F \cos \tau}{2\delta}. \quad (\text{C1})$$

Substituting  $v = 2(q - \delta)/3$  we get

$$v \approx -\frac{F \cos \theta}{3\delta}, \quad (\text{C2})$$

that should be compared to Eq. (14) of the main text for  $\gamma = \varkappa = \beta = 0$ .

With increasing value of  $F$  the absolute value of  $q_0$  also increases. When  $F$  reaches the critical point  $F = F_{\text{cr}}$  the value of  $q_0$  is given by  $|q_0| = \sqrt{F} = \sqrt{F_{\text{cr}}}$ . At this point the positive and the negative solution of Eq. (30) read

$$q(\tau) = \pm \sqrt{2F} \left| \sin \left( \frac{\tau}{2} \right) \right| = \pm \frac{\pi}{2} \left| \delta \sin \left( \frac{\tau}{2} \right) \right|, \quad (\text{C3})$$

while the velocity is given by

$$v = \frac{2\delta}{3} \left( \frac{\pi}{2} \left| \sin \frac{\theta}{2} \right| - 1 \right), \quad \text{for } F = F_{\text{cr}} \quad (\text{C4})$$

It is evident from Eq. (C3) that at  $F = F_{\text{cr}}$  the positive and the negative solution touch each other at the points  $\tau = 0$  and  $\tau = 2\pi$ . At these points one finds  $\tilde{q}_0 = 0$  and the positions of extrema coincide, hence there appear a possibility to jump between the two solutions from the stable point to the unstable one. With  $F$  increasing above  $F_{\text{cr}}$  the Eq. (32) of the main text no longer has any continuous solution. Therefore, for  $F > F_{\text{cr}}$ , one should search for a solution that is discontinuous:  $q = -\tilde{q}_0(\tau)$  for  $0 < \tau < \tau_0$  and  $q = \tilde{q}_0(\tau)$  for  $\tau_0 < \tau < 2\pi$ . At the discontinuity point  $\tau = \tau_0$  there exists a jump from the positive solution to the negative one. The negative solution changes back to the positive one at  $\tau = 2\pi$  so that the periodicity condition is fulfilled.

The discontinuity position is fixed by the condition  $\langle q \rangle = \delta$  that is written as

$$-\int_0^{\tau_0} d\tau \tilde{q}_0(\tau) + \int_{\tau_0}^{2\pi} d\tau \tilde{q}_0(\tau) = \delta. \quad (\text{C5})$$

Integrating the latter one finds Eq. (34) of the main text.

For  $F > F_{\text{cr}}$  the velocity reads

$$v = \frac{2}{3} \begin{cases} \sqrt{2F} \sin(\theta/2) - \delta, & 0 < \theta < \theta_0, \\ -\sqrt{2F} \sin(\theta/2) - \delta, & \theta_0 < \theta < 2\pi, \end{cases} \quad (\text{C6})$$

where the angle  $\theta_0 = -\tau_0$  obeys the relation  $\cos(\theta_0/2) = \sqrt{F_{\text{cr}}/F}$ .

## 2. Exact solution for $\gamma = \beta = 0$ and arbitrary $\varkappa$ .

In the absence of dispersion ( $\beta = 0$ ) the Eq. (25) simplifies to

$$\varkappa \dot{q} = q_0^2 - q^2 - F \cos \tau. \quad (\text{C7})$$

With the help of new variables

$$z = \tau/2, \quad q = \frac{\varkappa}{2y} \frac{dy}{dz}, \quad (\text{C8})$$

we rewrite Eq. (C7) in the canonical form of the Mathieu equation

$$\frac{\partial^2 y}{\partial \varphi^2} + [a - 2Q \cos(2\varphi)]y = 0, \quad (\text{C9})$$

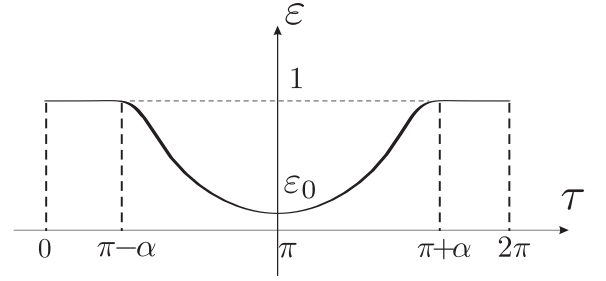


FIG. 4: Dependence of  $\varepsilon$  on  $\tau$  for  $\varkappa < \beta$ .

where  $a = -4\langle q^2 \rangle / \varkappa^2$  and  $Q = -2F / \varkappa^2$ .

The constraint  $\langle q \rangle = \delta$  can be rewritten in terms of the function  $y(z)$  as  $y(\pi) = \exp(2\pi\delta/\varkappa)y(0)$ . Thus, we get

$$\mu(a, Q) = 2i\delta/\varkappa, \quad (\text{C10})$$

where  $\mu(a, Q)$  is the Mathieu characteristic exponent. The parameter  $a$  is not a free external parameter but, in fact, has to be found self-consistently by calculating the average  $\langle q^2 \rangle$ . Instead of direct calculation of the average one may simply use Eq. (C10), which implicitly defines the dependence  $a(Q, \delta)$ .

Following this route one can express  $y$  in terms of the solution of Mathieu equation as follows

$$y(z) = G[a(Q, \delta), Q, z] = \text{MCos}[a(Q, \delta), Q, z] - i\text{MSin}[a(Q, \delta), Q, z], \quad (\text{C11})$$

where MCos and MSin are Mathieu cosine and sine, respectively. Using Eq. (C11) one can readily express the velocity  $v$  in terms of the angle  $\theta$  as

$$v(\theta) = -\frac{2}{3}\delta + \frac{2\varkappa}{3} \frac{\partial \ln[G[a(-2F/\varkappa^2, \delta), -2F/\varkappa^2, -\theta/2]]}{\partial \theta}. \quad (\text{C12})$$

The numerical analysis of this equation allows one to reproduce various regimes shown in Fig. 2. In the limit  $\varkappa \rightarrow 0$  we recover analytical solutions obtained above [see Eqs. (C2), (C4), and (C6)].

## Appendix D: Description of solitons in the limit $\beta \gg \varkappa$

For  $\beta \gg \varkappa$  the viscosity can be fully neglected. Let us consider the electron dynamics assuming for simplicity that  $\delta = 0$  and, as a consequence,  $F_{\text{cr}} = 0$ . In this case  $\delta\tau \simeq \varkappa/\sqrt{F}$  and  $\beta_0 \simeq \varkappa^2/\sqrt{F}$ . We assume that  $\varkappa \ll \sqrt{F}$  hence  $\delta\tau \ll 1$ . If the potential  $\tilde{U}(q)$  were static the electron energy would conserve. In fact, the potential slowly changes due to the variation of  $\tilde{q}_0$ , so that electron undergoes fast oscillations with the frequency of the order of  $\varkappa/\sqrt{\beta\beta_0} \sim \sqrt{\varkappa/\beta\delta\tau} \sim F^{1/4}/\beta^{1/2}$ , while its energy changes adiabatically.

Let us discuss this process in more detail. First, we consider what happens on the short time scales that are much shorter than the period of the external force. We introduce a dimensionless coordinate  $z$  and the energy  $\varepsilon$ :  $E = (2\tilde{q}_0^2/3)\varepsilon$ ,

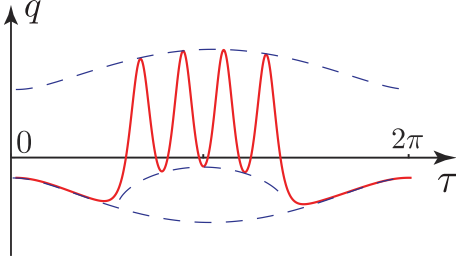


FIG. 5: Numerical simulation of oscillations of  $q$  for  $\kappa < \beta$  (red solid lines). Analytically calculated smooth envelopes are shown by dashed lines.

$q = \tilde{q}_0 z$ . Stable and unstable points of the potential correspond to  $\varepsilon = -1$  and  $\varepsilon = 1$ , respectively. Frequency of the electron oscillations in the potential depends on  $\varepsilon$ :  $\omega = \sqrt{2\tilde{q}_0/\beta} \Omega(\varepsilon)$  where

$$\frac{2\pi}{\Omega(\varepsilon)} = 2 \int_{z_1}^{z_2} \frac{dz}{H(\varepsilon, z)} \simeq \begin{cases} 2\pi, & \varepsilon = -1, \\ -\ln(1 - \varepsilon), & \varepsilon \rightarrow 1. \end{cases} \quad (\text{D1})$$

Here  $H(\varepsilon, z) = \sqrt{2\varepsilon/3 + z - z^3/3}$  and  $z_{1,2} = z_{1,2}(\varepsilon)$  are the turning points of the potential. The averaged value of the electron coordinate reads  $\langle q \rangle_\omega = \tilde{q}_0 f(\varepsilon)$ , where

$$f(\varepsilon) = \frac{\int_{z_1}^{z_2} dz z H^{-1}(\varepsilon, z)}{\int_{z_1}^{z_2} dz H^{-1}(\varepsilon, z)} \begin{cases} 1, & \varepsilon = -1, \\ -1, & \varepsilon = 1, \end{cases} \quad (\text{D2})$$

and  $\langle \dots \rangle_\omega$  stands for the averaging over the fast oscillations with the frequency  $\omega(\varepsilon)$ . Simple numerical analysis shows that  $f(\varepsilon)$  is very well approximated by  $f(\varepsilon) \approx -1 + 2^{6/7}(1 - \varepsilon)^{1/7}$ .

Next, we study slow dynamics caused by a time dependence of  $\tilde{q}_0$ . In this case it is useful to define an adiabatic invariant  $J(\varepsilon) = \oint p dq = J(1)j(\varepsilon)$ , where  $J(1) = (24\sqrt{2}/5)\sqrt{\beta}\tilde{q}_0^{5/2}$  and

$$j(\varepsilon) = \frac{5}{12} \int_{z_1}^{z_2} dz H(\varepsilon, z) \simeq \begin{cases} \frac{5\pi(1+\varepsilon)}{36}, & \varepsilon \rightarrow -1, \\ 1, & \varepsilon = 1. \end{cases} \quad (\text{D3})$$

Numerically one can approximate  $j(\varepsilon) \approx (1 + \varepsilon)/2$ .

We parameterize  $q_0 = AF$ , where  $A$  is a dimensionless constant hence  $\tilde{q}_0 \approx \sqrt{F}\sqrt{A - \cos(\tau)}$ . We also parameterize the energy at the time  $\tau = \pi$  as  $\varepsilon_0$ . From the conservation of the adiabatic invariant we, therefore, conclude that the dependence of energy on time is implicitly given by the following equation

$$[A - \cos(\tau)]^{5/4} j(\varepsilon) = [A + 1]^{5/4} j(\varepsilon_0). \quad (\text{D4})$$

The dependence of  $\varepsilon$  on  $\tau$  that follows from Eq. (D4) is shown at Fig. 4.

At  $\tau \approx \pi \pm \alpha$  the energy approaches the limiting value  $\varepsilon = 1$  and sticks to this point because  $\Omega(1) = 0$  [see Eq. (D1)]. In

this regime the value of  $q$  is given by  $-\tilde{q}_0$ . From Eq. (D4), we find the relation between  $\alpha$  and  $j(\varepsilon_0)$  as

$$j(\varepsilon_0) \approx \left[ \frac{A + \cos(\alpha)}{A + 1} \right]^{5/4}. \quad (\text{D5})$$

At this point we have to take advantage of the constraint  $\langle q \rangle = 0$ . To find the value of  $\langle q \rangle$  one should average  $\langle q \rangle_\omega$  over slow oscillations of the external field. This yields the following condition

$$\int_{\pi}^{\pi+\alpha} d\tau \tilde{q}_0(\tau) f(\varepsilon(\tau)) + \int_{\pi+\alpha}^{2\pi} d\tau [-\tilde{q}_0(\tau)] = 0, \quad (\text{D6})$$

that allows one to determine  $\alpha$ . In particular, replacing the functions  $f(\varepsilon)$  and  $j(\varepsilon)$  in Eqs. (D4) and (D6) with the corresponding approximative formulas, one arrives at the following equation for  $\alpha$

$$\int_0^\alpha dx \sqrt{A + \cos x} \left\{ -1 + 2 \left( 1 - \left[ \frac{A + \cos(\alpha)}{A + 1} \right]^{5/4} \right)^{1/7} \right\} = \int_\alpha^\pi dx \sqrt{A + \cos x}. \quad (\text{D7})$$

Once the value of  $\alpha$  is found one can use Eq. (D5) to determine  $\varepsilon_0$ . Parameter  $A$  can be obtained from the numerical solution of hydrodynamical equations,  $A \gtrsim 1$ . Simple numerical analysis of Eq. (D6) yields

$$\alpha \approx 1.3, \quad \varepsilon_0 \approx 0.13. \quad (\text{D8})$$

The qualitative behavior of the function  $q(\tau)$  is illustrated in Fig. S2.

The values given in Eq. (D7) appear to be in a very good agreement with the solution obtained by direct numerical simulation of the original hydrodynamic equations. Below, we briefly describe the numerical method.

## Appendix E: Numerical solution of hydrodynamic equations

In this section, we analyze the most general case of non-stationary hydrodynamic equations in the presence of dispersion, viscosity, and disorder-induced friction. In the rotating reference frame ( $t' = t$  and  $\theta = \varphi - \omega t$ ), these equations read

$$\frac{\partial n}{\partial t'} + \frac{\partial}{\partial \theta} [(1 + n)v - \omega n] = 0, \quad (\text{E1})$$

$$\frac{\partial v}{\partial t'} + \frac{\partial}{\partial \theta} \left[ \frac{v^2}{2} - v\omega + \omega_0^2 n - \kappa \frac{\partial v}{\partial \theta} + \beta \frac{\partial^2 v}{\partial \theta^2} \right] = -\gamma v + \frac{eE_0}{mR} \sin \theta, \quad (\text{E2})$$

For the resonance approximation,  $\delta \ll \omega_0$ , the solution to these equation is very close to a stationary solution in the rotating reference frame. In the other words, we may assume that derivatives  $\partial/\partial t'$  are on the order of  $\delta$  and, therefore, are



small compared to  $\omega$ . Then, Eqs. (E1) and (E2) can be somewhat simplified. As the first step we rewrite Eq. (E1) as

$$\frac{\partial n}{\partial \theta} = \frac{1}{\omega} \left[ \frac{\partial n}{\partial t'} + \frac{\partial(1+n)v}{\partial \theta} \right]. \quad (\text{E3})$$

In the next step we substitute  $n \approx v/\omega$  into the r.h.s. of this equation. As a result, we obtain a closed non-stationary equation for the velocity

$$2 \frac{\partial v}{\partial t'} + \frac{\partial}{\partial \theta} \left[ \frac{3}{2} v^2 + 2\delta v - \varkappa \frac{\partial v}{\partial \theta} + \beta \frac{\partial^2 v}{\partial \theta^2} \right] = -\gamma v + \frac{eE_0}{mR} \sin \theta, \quad (\text{E4})$$

which is easily solved by the standard built-in realization of the finite-element method in Mathematica. For sufficiently small  $\gamma$  and for  $\varkappa \ll \sqrt{F}$ ,  $\beta \ll \sqrt{F}$  we find the solution to be stationary in the rotating reference frame at sufficiently long times. This reproduces the results that are shown in Figs. 2,3. Also, in the limit  $\beta_0 < \beta < \varkappa$  the numerical simulations yield the values of  $\alpha$  and  $\varepsilon_0$ , which are in a very good agreement with those listed in Eq. (D8).

- 
- [1] J.B. Khurgin, *Nature Nanotechnology* **10**, 2 (2015).
  - [2] P. Nordlander, *Nature Nanotechnology* **8**, 76 (2013).
  - [3] J. Heber, *Nature Materials* **11**, 745 (2012).
  - [4] A. N. Grigorenko, M. Polini, K. S. Novoselov, *Nature Photonics* **6**, 749 (2012).
  - [5] F. H. L. Koppens, D. E. Chang, F. J. Garcia de Abajo, *Nano Lett.* **11**, 3370 (2011).
  - [6] D. K. Gramotnev and S. I. Bozhevolnyi, *Nature Photonics* **4**, 83 (2010).
  - [7] S. A. Maier, *Plasmonics: Fundamentals and Applications* (Springer, 2007).
  - [8] R. N. Gurzhi, *Usp. Fiz. Nauk* **94**, 689 (1968) [*Sov. Phys. Usp.* **11**, 255 (1968)].
  - [9] M. J. M. de Jong, L. W. Molenkamp, *Phys. Rev. B* **51**, 13389 (1985).
  - [10] R. Jaggi, *J. Appl. Phys.* **69**, 816 (1991).
  - [11] R. N. Gurzhi, A. N. Kalinenko, and A. I. Kopeliovich, *Phys. Rev. Lett.* **72**, 3872 (1995).
  - [12] K. Damle, S. Sachdev, *Phys. Rev. B* **56**, 8714 (1997).
  - [13] H. Buhmann, L. W. Molenkamp, R. N. Gurzhi, A. N. Kalinenko, A. I. Kopeliovich and A. V. Yanovsky, *Low Temp. Phys.* **24**, 737 (1998).
  - [14] H. Predel, H. Buhmann, L. W. Molenkamp, R. N. Gurzhi, A. N. Kalinenko, A. I. Kopeliovich, and A. V. Yanovsky, *Phys. Rev. B* **62**, 2057 (2000).
  - [15] A. V. Andreev, S. A. Kivelson, and B. Spivak, *Phys. Rev. Lett.* **106**, 256804 (2011).
  - [16] D. Forcella, J. Zaanen, D. Valentinis, and D. van der Marel, *Phys. Rev. B* **90**, 035143 (2014).
  - [17] A. Tomadin, G. Vignale, and M. Polini, *Phys. Rev. Lett.* **113**, 235901 (2014).
  - [18] P. S. Alekseev, arXiv:1603.04587v1 (2016).
  - [19] A. B. Kashuba, *Phys. Rev. B* **78**, 085415 (2008).
  - [20] L. Fritz, J. Schmalian, M. Müller, and S. Sachdev, *Phys. Rev. B* **78**, 085416 (2008).
  - [21] M. Müller, J. Schmalian, and L. Fritz, *Phys. Rev. Lett.* **103**, 025301 (2009).
  - [22] M. Mendoza, H. J. Herrmann, and S. Succi, *Phys. Rev. Lett.* **106**, 156601 (2011).
  - [23] B. N. Narozhny, I. V. Gornyi, M. Titov, M. Schütt, and A. D. Mirlin, *Phys. Rev. B* **91**, 035414 (2015).
  - [24] A. Cortijo, Y. Ferreirós, K. Landsteiner, and M. A. H. Vozmediano, *Phys. Rev. Lett.* **115**, 177202 (2015).
  - [25] M. I. Dyakonov and M. S. Shur, *Phys. Rev. Lett.* **71**, 2465 (1993).
  - [26] M. I. Dyakonov and M. S. Shur, *Phys. Rev. B* **51**, 14341 (1995).
  - [27] M. I. Dyakonov and M. S. Shur, *IEEE Trans. on Elec. Dev.* **43**, 380 (1996).
  - [28] A. P. Dmitriev, A. S. Furman, and V. Yu. Kachorovskii, *Phys. Rev. B* **54**, 14020 (1996).
  - [29] A. P. Dmitriev, A. S. Furman, V. Yu. Kachorovskii, G. G. Samsonidze, and Ge. G. Samsonidze, *Phys. Rev. B* **55**, 10319 (1997).
  - [30] T. Otsuji and M. S. Shur, *IEEE Microwave Magazine*, **15**, 43 (2014).
  - [31] W. Knap, D. B. But, N. Dyakonova, D. Coquillat, A. Gutin, O. Klimenko, S. Blin, F. Teppe, M. S. Shur, T. Nagatsuma, S. D. Ganichev, and T. Otsuji, *Recent Results on Broadband Nanotransistor Based THz Detectors* in NATO Science for Peace and Security Series B, Physics and Biophysics: THz and Security Applications, edited by C. Corsi, F. Sizov, (Springer, Dordrecht, Netherlands, 2014).
  - [32] D. Veksler, F. Teppe, A. P. Dmitriev, V. Yu. Kachorovskii, W. Knap, M. S. Shur, *Phys. Rev. B* **73**, 125328 (2006).
  - [33] G. C. Dyer, G. R. Aizin, S. Preu, N. Q. Vinh, S. J. Allen, J. L. Reno, and E. A. Shaner, *Phys. Rev. Lett.* **109**, 126803 (2012).
  - [34] G. R. Aizin, G. C. Dyer, *Phys. Rev. B* **86**, 235316 (2012).
  - [35] V. Yu. Kachorovskii and M. S. Shur, *Appl. Phys. Lett.* **100**, 232108 (2012).
  - [36] G. C. Dyer, G. R. Aizin, S. James Allen, A. D. Grine, D. Bethke, J. L. Reno, and E. A. Shaner, *Nature Photonics* **7**, 925 (2013).
  - [37] L. Wang, X. Chen, W. Hu, A. Yu, and W. Lu, *Appl. Phys. Lett.* **102**, 243507 (2013).
  - [38] X. G. Peralta, S. J. Allen, M. C. Wanke, N. E. Harff, J. A. Simmons, M. P. Lilly, J. L. Reno, P. J. Burke, and J. P. Eisenstein, *Appl. Phys. Lett.* **81**, 1627 (2002).
  - [39] E. A. Shaner, M. Lee, M. C. Wanke, A. D. Grine, J. L. Reno, and S. J. Allen, *Appl. Phys. Lett.* **87**, 193507 (2005).
  - [40] E. A. Shaner, M. C. Wanke, A. D. Grine, S. K. Lyo, J. L. Reno, and S. J. Allen, *Appl. Phys. Lett.* **90**, 181127 (2007).
  - [41] A. V. Muravjov, D. B. Veksler, V. V. Popov, O. V. Polischuk, N. Pala, X. Hu, R. Gaska, H. Saxena, R. E. Peale, and M. S. Shur, *Appl. Phys. Lett.* **96**, 042105 (2010).
  - [42] G. C. Dyer, S. Preu, G. R. Aizin, J. Mikalopas, A. D. Grine, J. L. Reno, J. M. Hensley, N. Q. Vinh, A. C. Gossard, M. S. Sherwin, S. J. Allen, and E. A. Shaner, *Appl. Phys. Lett.*, **100**, 083506 (2012).
  - [43] G. R. Aizin, V. V. Popov, and O. V. Polischuk, *Appl. Phys. Lett.* **89**, 143512 (2006).
  - [44] G. R. Aizin, D. V. Fateev, G. M. Tsymbalov, and V. V. Popov, *Appl. Phys. Lett.* **91**, 163507 (2007).

- [45] T.V. Teperik, F.J. Garcí'a de Abajo, V.V. Popov, and M. S. Shur, Appl. Phys. Lett. **90**, 251910 (2007).
- [46] V. V. Popov, D. V. Fateev, T. Otsuji, Y. M. Meziani, D. Coquillat, and W. Knap, Appl. Phys. Lett. **99**, 243504 (2011).
- [47] Y. M. Meziani, H. Handa, W. Knap, T. Otsuji, E. Sano, V. V. Popov, G. M. Tsymbalov, D. Coquillat, and F. Teppe, Appl. Phys. Lett. **92**, 201108 (2008).
- [48] T. Otsuji, Y. M. Meziani, T. Nishimura, T. Suemitsu, W. Knap, E. Sano, T. Asano, and V. V. Popov, J. Phys.: Condens. Matter **20**, 384206 (2008).
- [49] E. L. Ivchenko and S. D. Ganichev, Pisma v ZheTF **93**, 752 (2011) [JETP Lett. **93**, 673 (2011)].
- [50] I. V. Rozhansky, V. Yu. Kachorovskii, and M. S. Shur, Phys. Rev. Lett. **114**, 246601 (2015).
- [51] O. V. Kibis, Phys. Rev. Lett. **107**, 106802 (2011).
- [52] O. V. Kibis, O. Kyriienko, I. A. Shelykh, Phys. Rev. B **87**, 245437 (2013).
- [53] A. M. Alexeev, I. A. Shelykh, M. E. Portnoi, Phys. Rev. B **88**, 085429 (2013).
- [54] F. K. Joibari, Ya. M. Blanter, G. E. W. Bauer, Phys. Rev. B **90**, 155301 (2014).
- [55] A. M. Alexeev, M. E. Portnoi, Phys. Rev. B **85**, 245419 (2012).
- [56] V. V. Kruglyak, M. E. Portnoi, Technical Physics Letters **31**, 1047 (2005) [Pis'ma v Zh. Tekh. Fiziki **31**, 20 (2005)].
- [57] V. V. Kruglyak, M. E. Portnoi, R. J. Hicken, Journal of Nanophotonics **1**, 013502 (2007).
- [58] K. L. Koshelev, V. Yu. Kachorovskii, and M. Titov, Phys. Rev. B **92**, 235426 (2015).
- [59] I. V. Protopopov, D. B. Gutman, P. Schmitteckert, A. D. Mirlin, Phys. Rev. B **87**, 045112, (2013).
- [60] I. V. Protopopov, D. B. Gutman, M. Oldenburg, A. D. Mirlin, Phys. Rev. B **89**, 161104 (2014).
- [61] L. P. Pitaevskii, Sov. Phys. JETP **12**, 1008 (1961).
- [62] J. P. van der Ziel, P. S. Pershan and L. D. Malmstrom, Phys. Rev. Lett. **15**, 190 (1965).
- [63] A. V. Kimel, A. Kirilyuk, P. A. Usachev, R. V. Pisarev, A. M. Balbashov and Th. Rasing, Nature **435**, 655 (2005).
- [64] V. I. Belotelov, L. L. Doskolovich, A. K. Zvezdin, Phys. Rev. B **98**, 077401 (2007).
- [65] A. Kirilyuk, A. V. Kimel, and T. Rasing, Rev. Mod. Phys. **82**, 2731 (2010).
- [66] A. Kirilyuk, A. V. Kimel and Th. Rasing, Phil. Trans. R. Soc. A **369**, 3631 (2011).
- [67] M. L. Polianski, Phys. Rev. B **80**, 241301(R) (2009).
- [68] T. J. Yen, W. J. Padilla, N. Fang, D. C. Vier, D. R. Smith, J. B. Pendry, D. N. Basov, X. Zhang, Science **303**, 1494 (2004).
- [69] L. D. Landau and E. M. Lifshitz, *Course of Theoretical Physics: Fluid Mechanics*, (Pergamon, New York, 1987).